# The effect of porosity on fragmentation statistics of dynamically loaded $ZrO_2$ ceramics

Marina Davydova, Sergei Uvarov, Oleg Naimark
*Institute of Continuous Media Mechanics Ural Branch Russian Academy of Sciences, 1, Ac. Korolev str., Perm 614013, Russia.*
*1957davydova@gmail.com, http://lab13.icmm.ru/index.php/en/*
*pia@icmm.ru, http://lab13.icmm.ru/index.php/en/*
*naimark@icmm.ru, http://lab13.icmm.ru/index.php/en/*

**ABSTRACT.** The effect of load intensity and porous material structure on the fragmentation statistics of $ZrO_2$(MgO)-based ceramics is studied. Cylindrical samples were fragmented under dynamic compression. Experimental data processing showed that the shape of stress-strain curves, the fragment size distribution and distribution of time intervals between the fractoluminiscense impulses depend on the sample porosity and load intensity. The X-ray Computed Tomography (CT) study of porous material structures allowed us to link the fragmentation statistics with pronounced porosity clustering (about 97% of the total pore volume) formed due to sintering.

**KEYWORDS.** Fragmentation; Ceramic; Crack cluster.

**Citation:** Davydova, M., Uvarov, S., Naimark, O., The effect of sample porosity on statistical regularities of dynamical fragmentation of ceramic $ZrO_2$, Frattura ed Integrità Strutturale, 43 (2018) 106-112.

**Received:** 17.10.2017
**Accepted:** 28.10.2017
**Published:** 01.01.2018



## INTRODUCTION

Synthesis of ceramic materials with projected properties implies studying the relationship between physical and mechanical characteristics and porosity of the material. On the one hand, the role of porosity as the main structural factor is associated with the absence of the effective mechanism of structural relaxation due to a dislocation motion, and, on the other hand, with the long–range interactions in the ensemble of pores growing during the deformation. These features determine the pore clustering, damage-failure kinetics and mechanical properties in a wide range of load intensity [1]. Study of the effect of porosity revealed the influence of the porous cluster morphology on the deformation properties of ceramics $ZrO_2(Y_2O_3)$ [1,2]. This is associated with a change in pore distributions related to the transition from the isolated pore structure to the structure with pore clustering. In this paper, the effect of pore cluster morphology of the ceramic material subject to dynamic loading and fragmentation was studied based on the analysis of 2D and 3D structure images obtained by X-ray Computed Tomography (CT).

## SAMPLES AND EXPERIMENTAL TECHNIQUE

The samples used in the experiment were fabricated at the Institute of Strength Physics and Material Sciences (SB RAS, Tomsk) from the ceramics of $ZrO_2$-MgO system (8.6 % mol MgO) by the plasmochemical method [4]. The manufacture of ceramic samples was carried out by powder metallurgy technique, which consisted in powder

compacting within the steel molds with a hydraulic punch under compacting pressure of 70 MPa. The obtained compacts were sintered in air at 1550°C and then subjected to isothermal exposure within an hour. The samples had the shape of cylinders of diameter from 8.5 to 13 mm, length from 6.8 to 12.2 mm and weight from 2.2 to 6.3g. Porosity of the initial powder before compacting varied from 10% to 60%.

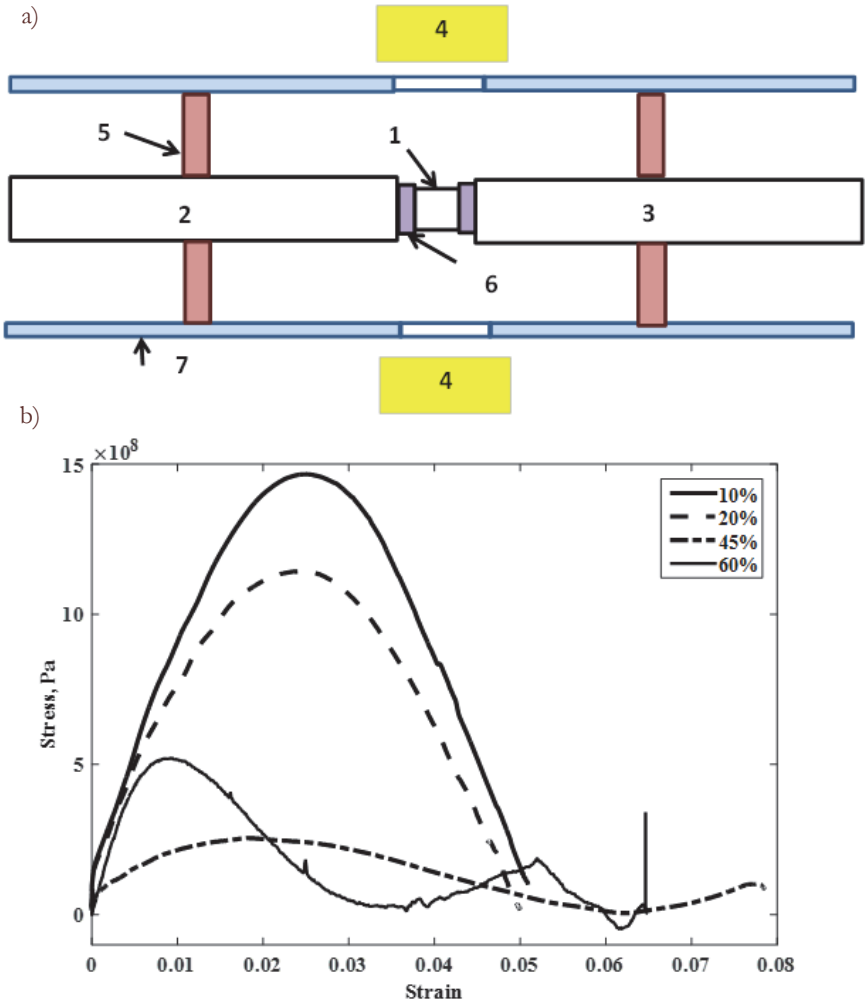


Figure 1: a) The scheme of experimental set-up (1-sample, 2-input bar, 3-output bar, 4-photomultiplier tube (PMT), 5- teflon ring, 6-impedance matched WC insert, 7- plastic cylinder); b) stress-strain curve for ceramic samples with porosity of 10%, 20%, 45%, 60%.

Dynamic tests were carried out using a split Hopkinson pressure bar, (Fig.1(a)), which consists of the input (3 m in length and 25 mm in diameter) and output (1 m in length and 25 mm in diameter) bars to provide single-pulse loading conditions. The bars were made of high-strength steel ($\sigma_B \sim 1900GPa$). A sample was sandwiched between the bars and separated from them by the impedance–matched tungsten carbide (WC) inserts, which prevented samples from being indented into the bars, the hardness of which was less than the hardness of the examined ceramics. The position of the bars was carefully adjusted before each loading to ensure a uniform distribution of the force applied to the end faces of the samples. In order to eliminate the effect of dispersion in the bars and to provide the dynamic stress equilibrium conditions (the equality of forces applied to the specimen ends) during tests, we used a brass pulse shaper, which was a 7x7 mm plate of thickness 1.4 mm. By varying the striker velocity, we managed to increase the deformation rate from 400 to 3000 $s^{-1}$.

The study of fragmentation statistics (fragment size distribution and distribution of time intervals between the fractoluminiscence impulses) required modification of the traditional scheme of the split Hopkinson bar. The samples and the ends of the bars adjacent to the samples were placed into plastic cylinders, which allowed the fragments of ceramics to remain confined within the cylinder and provided dimming necessary for registration of the fractoluminiscence impulses. The formation of fracture surfaces during sample fragmentation initiated light emission, which was recorded by the two

photomultiplier tubes (PMT) with the rise time of 0.8 ns, which were located at the opposite lateral surfaces of the sample. To improve reliability of experiments, two PMT were used. From the PMT signal was transmitted to the Tektronix digital oscilloscope DP07254 with a band width of 3.5 GHz and sampling rate less than 10 GHz. Thus, the modified setup had the advantage of getting both the deformation curves and the statistic characteristics of the fragmentation process, based on the data on the two types of distribution: size distribution of the spatial parameter (fragment size) and size distribution of the temporal parameter (the interval between fractoluminiscence impulses).

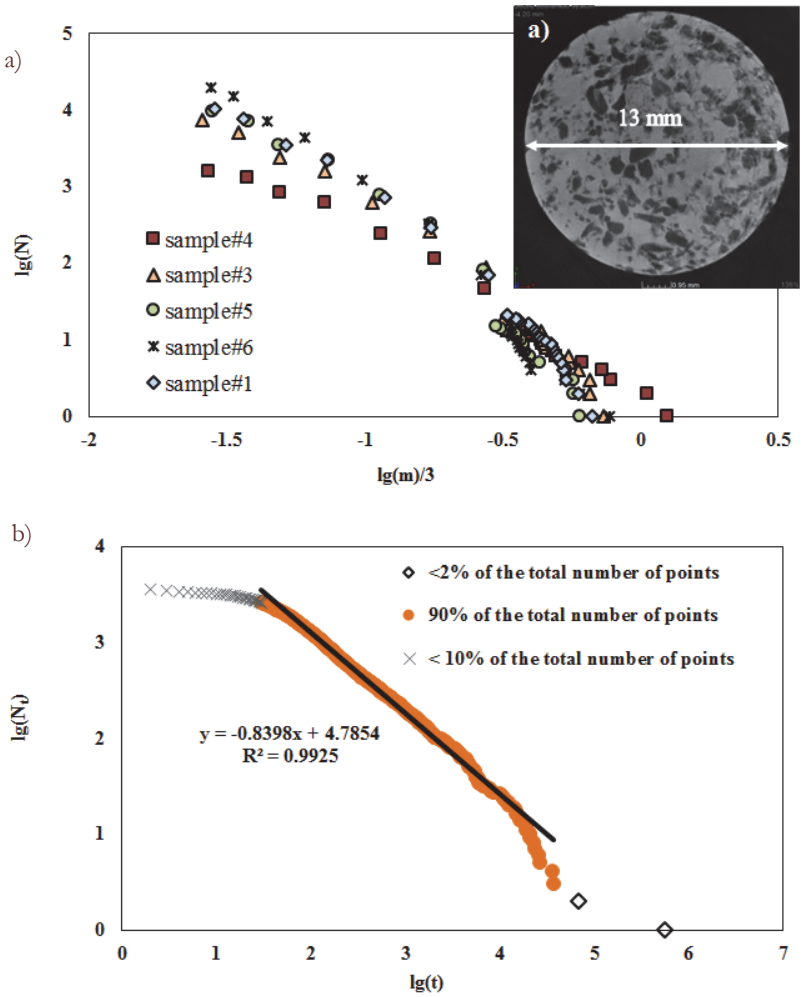


Figure 2: Sample with porosity of 30%: a) CT image of the sample cross section; b) fragment size distribution function for 5 specimens; c) typical time interval distribution function.

## DYNAMIC FRAGMENTATION RESULTS

Fig. 1(b) shows typical stress-strain curves for ceramic samples with different porosity before sintering. It should be noted that for the samples with porosity less than 45%, the stress-strain $(\sigma - \varepsilon)$ curves have one stress maximum, whereas for the samples with porosity of 45% and 60% the $(\sigma - \varepsilon)$ curves show two maxima.

The experimental data were used to construct the cumulative fragment size distribution, i.e., the relationships between the number of fragments, $N$, the size (mass) of which is larger than a prescribed value, and the size, $r$ (mass $m$), of the fragment. The fragment mass was measured by weighing fragments on the electronic balance HR-202i. Fig. 2(b) and Fig. 3(b) present the log-log plots of the cumulative fragment size distribution for the samples, in which the initial porosity of the powder component was 20%, (Fig. 2(b)), and 60%, (Fig. 3(b)). The above distributions are well described ($R^2$>0.96) by the power law function:

$$N \cong Cr^{-D_S} \tag{1}$$

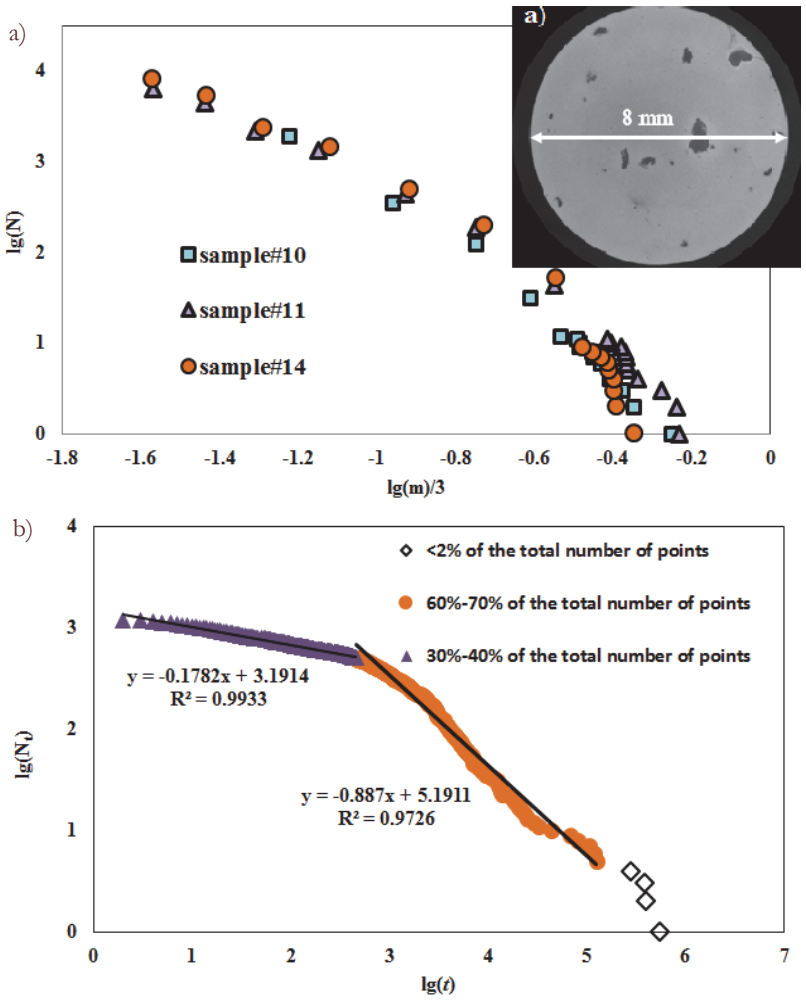


Figure 3: Sample with porosity 2 %: a) CT image of the sample cross section; b) fragment size distribution function for 3 samples; c) typical time interval distribution function.

The value of the power law exponent $D_S$ depends on the material porosity and load intensity. The time intervals between the fractoluminiscence impulses was about 2÷$10^3$ ns in the active fracture stage, while in the final stage it increased up to $10^6$ ns. The change in porosity from 10% to 60% led to a growth of the impulse number by a factor of 18. Fig. 2(c) and Fig. 3(c) present the log-log-plots of the time interval distribution function, which depicts the dependence of the number of intervals, $N_t$, with the size larger than or equal to $t$. The distribution function for the samples with porosity of 10÷45% is well described ($R^2$>97%) by two power laws (two straight lines), (Fig. 3(c)). Whereas for the samples with porosity of 60% it is described by power law (one straight line), (Fig. 2(c)):

$$N_t \cong C_1 t^{-D_t} \tag{2}$$

The value of power law exponent $D_t$ in the relation (2) is affected by the porosity and load value.

The ceramic material under study has a cellular structure, which is formed by hollow powder particles (particle porosity) separated by interparticle pores [3,4]. Therefore, it was suggested in [5] that the difference in the time interval distribution functions, (Fig. 2(c) and Fig. 3(c)), for samples of different porosity and a weak sensitivity of the power law exponent to load intensity for low porosity samples, (Fig. 3(b)), should be explained by the competition between two pore systems. The

study of porous structure of the non-deformed samples using X-ray Computed Tomography (CT) indicates that the key role in fracture and fragmentation process for studying ceramic is belong to the interparticle pores system.

## X-RAY COMPUTED TOMOGRAPHY (CT) STUDY

The investigation of porous structure (inter-particle porosity) of ceramic samples with initial powder porosity of 20% and 60% was done using X-ray Computed Tomography (Nikon Metrology XT H 225+180 LC, Perm State University). The CT data obtained for the sample with initial porosity of 60% (diameter is 13 mm and height is 12 mm) were represented by a stack of 1039 cross-section images of the sample, (Fig.2(a)), and for the sample with initial porosity of 20% (diameter is 8 mm and height is 7 mm) – by a stack of 1350 images, (Fig.3(a)). Dark areas in Fig.2(a) and Fig.3(a) correspond to pores. Processing of the CT data was done using the ImageJ (IJ1.46r) open source software, which allowed us to calculate the number and volume of the pores, porosity, area and perimeter of the pores in all slices and to perform 3D visualization. The results of stack processing showed that the real porosity of the sample produced from the powder with initial porosity of about 60% was 30% and the real porosity of the sample with initial powder porosity of about 30% was 2%. The cumulative pore size distribution function for the pore size greater than a prescribed value is presented in Fig.4. In the calculation we used the stack of 1350 slices in the case of 2% porosity sample and the stack of 900 slices in the case of 30% porosity sample. Gray dots indicate the pore size distribution for the low porosity (2%) sample. The pore size distribution for the sample with porosity of 30% is described by a curve consisting of orange dots and separately located big red dot. The construction of 3D images, (Fig.5 and Fig.6), of the sample pore structure allowed us to establish that volume of 374 $mm^3$ (red dot) is the pore cluster, and the orange curve describes the size distribution of pores that stand alone (outside the cluster). Moreover, cluster covers 98% of porosity and this is the main reason of its considerable influence on the fracture process. Note that it will be impossible to obtain the above cluster if we try to construct 3D image of the pore ensemble using a small number of slices, (10 or 20, Fig.6(a)): the formation of 3D cluster is feasible only with a sufficiently large number of slices, (more than 100, Fig. 6(b)).

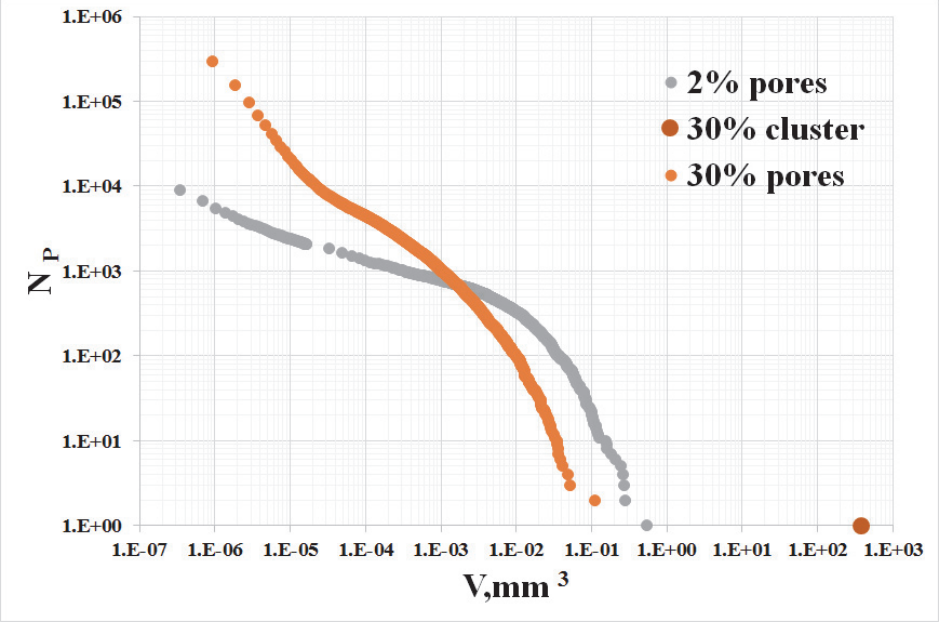


Figure 4: Cumulative pore size distribution functions for samples with porosity 2 % and 30%

## CONCLUSION

The experiments on dynamical fragmentation of $ZrO_2$ ceramics showed, that the initial porosity of the samples has effect on the shape of the stress-strain curves, (Fig. 1(b)), the scatter of the power law exponent of the fragment size distribution, (Fig. 2(b) and Fig.3(b)), and the type of the time interval distribution function, (Fig. 2(c), Fig. 3(c)).

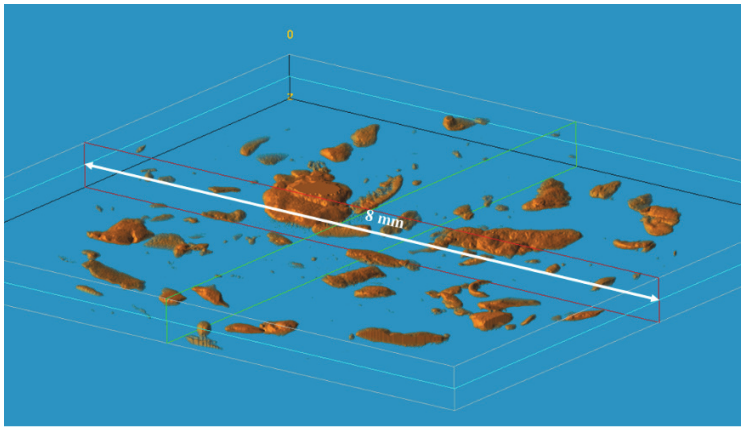


Figure 5: 3D image of the pore system for 2% porosity sample (100 slices).

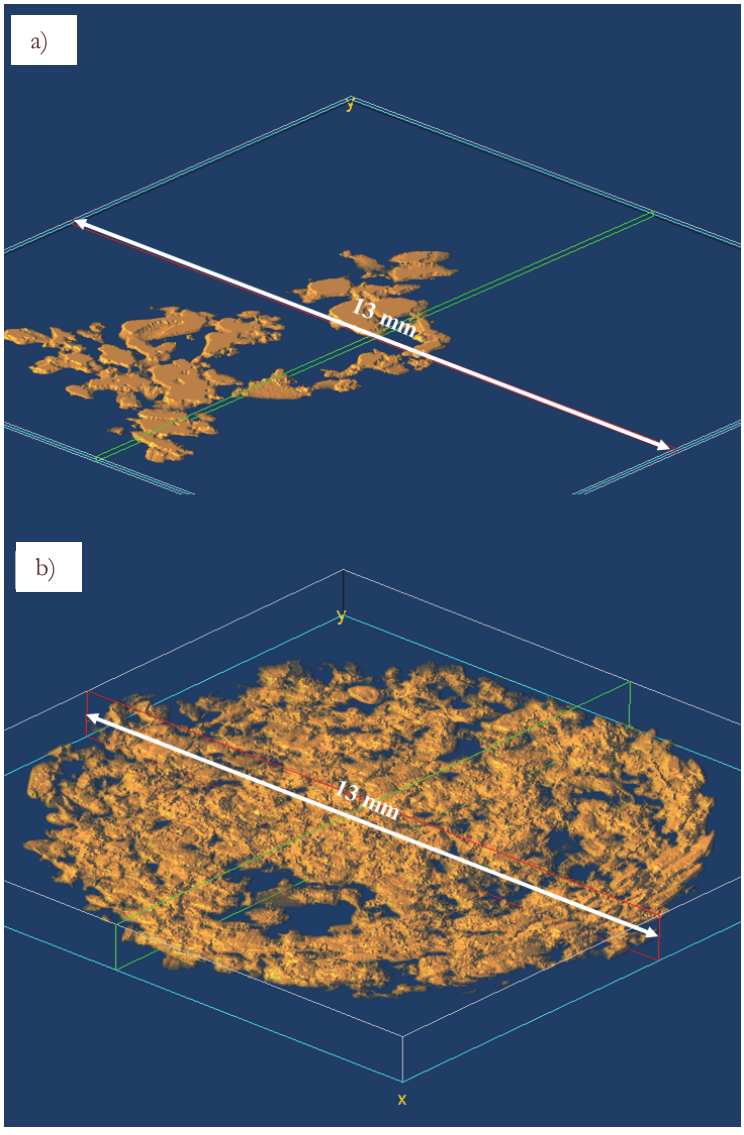


Figure 6: 3D image of the pore cluster for 30% porosity sample: a) 10 slices; b) 100 slices.

Processing of CT images of non-deformed samples using the ImageJ code allowed us to conclude, that mentioned features of ceramics fragmentation with different porosity should be associated with a large cluster, which is formed in the process of preparation of ceramic samples with porosity of 30% (from the initial powder compact with 60% porosity) and combines up to 98% of all sample pores.

Initial fracture stage, which involves multiple initiation and growth of porous defects plays the key role in fragmentation of sample with low porosity 2% (initial 20%). But for the samples with 30% porosity (initial 60%), this stage is practically absent due to the presence of pore cluster, and the failure is caused by the loss of stability of the partitions between the pores. This hypothesis is confirmed by the following facts:

- stress-strain curves for high porosity samples have two maxima, the first of which corresponds to the pore collapse and the second - to the deformation of compacted material;
- in the initial stage of fracture, the intervals between the fractoluminescence impulses for the sample with 2% porosity are two or three times longer than for the sample with 30% porosity.

The increase in porosity from 2% to 30% leads to an 18-fold growth of the number of fractoluminescence impulses, which corresponds to the scale-invariant power law distribution of time intervals (straight line in Fig. 2(c)). The scatter of power law exponent (Fig. 2(b)) for the sample with 30% porosity is also due to the formation of a cluster, which provides a wide range of possible fracture variants.

The scale invariant law associated with the increase of porosity is also the fundamental subject of research, because it characterizes the material ability to demonstrate the criticality of damage-failure transition due to the involvement of total spectra of the space-time scales into the mechanisms of the defect-induced structural relaxation. The established characteristic features of fragmentation may be crucial for studying the absorption mechanisms [6,7], which can exhibit scaling (structural wave fronts [8]) in a wide range of load intensity.

## REFERENCES

[1] Buyakova, S.P., Maslovskii, V.L., Nikitin, D.S., Kulkov, S.N., Mechanical instability of a porous material, Technical Physics Letters, 27(12) (2001) 981-983. DOI: 10.1134/1.1432322

[2] Kulkov, S.N., Maslovskii, V.L., Buyakova, S.P., Nikitin, D.S., The non-Hooke's behavior of porous zirconia subjected to high-rate compressive deformation, Technical Physics. The Russian Journal of Applied Physics., 47(3) (2002) 320-324. DOI: https://doi.org/10.1134/1.1463121

[3] Buyakova, S. P., Kulkov, S. N., Effect of mechanical processing of ultrafine $ZRO_2$ + 3 wt % MgO powder on the microstructure of ceramics produced from it, Inorganic Materials, 46 (2010) 1155–1158. DOI:10.1134/S0020168510100249

[4] Kalatur, E.S., Kozlova, A.V., Buyakova, S.P., Kulkov, S.N., Deformation behavior of zirconia-based porous ceramics, IOP Conf. Series: Materials Science and Engineering, 47 (2013) P.012004. DOI: 10.1088/1757-899X/47/1/012004.

[5] Davydova, M.M., Uvarov, S.V., Naimark, O.B., Space-time scale invariance under dynamic fragmentation of quasi-brittle materials, Phys. Mesomechanics, 19(1) (2016) 86-92. DOI: 10.1134/S1029959916010094.

[6] Naimark, O.B., Some regularities of scaling in plasticity, fracture, and turbulence, Phys. Mesomechanics, 19(3) (2016) 307-318. DOI: 10.1134/S1029959916030097.

[7] Naimark, O.B., Defect induced transitions as mechanisms of plasticity and failure in multifield continua in: G. Capriz, P. M. Mariano (Eds.), Advances in Multifield Theories of Continua with Substructure, Birkhäuser, Boston, (2004) 75-114. DOI: https://doi.org/10.1007/978-0-8176-8158-6.

[8] Grady, D., Structured shock waves and the fourth-power law, J. of Applied Physics, 107 (2010) 013506. DOI: http://dx.doi.org/10.1063/1.3269720.